Layer-to-Layer Height Control for Laser Metal Deposition Processes

Lie Tang, Jianzhong Ruan, Todd E. Sparks, Robert G. Landers, and Frank Liou

Missouri University of S&T

Department of Mechanical and Aerospace Engineering

1870 Miner Circle, Rolla, Missouri 65409–0050

{ltx8d;jzruan;tsparks;landersr;liou}@mst.edu

Abstract **Reviewed, accepted September 10, 2008**

A Laser Metal Deposition (LMD) height controller design methodology is presented in this paper. The height controller utilizes the Particle Swarm Optimization (PSO) algorithm to estimate model parameters between layers using measured temperature and track height profiles. The process model parameters for the next layer are then predicted using Exponentially Weighted Moving Average (EWMA). Using the predicted model, the powder flow rate reference profile, which will produce the desired layer height reference, is then generated using Iterative Learning Control (ILC). The model parameter estimation capability is tested using a four-layer deposition. The results demonstrate the simulation based upon estimated process parameters matches the experimental results quite well. Simulation study also shows that the methodology described above works well in producing the reference layer height.

1. Introduction

Laser Metal Deposition (LMD) is an important Solid Freeform Fabrication (SFF) technology which allows functionally graded metal parts to be deposited from three dimensional computer models [1]. Unlike traditional machining operations which build parts by material subtraction, LMD is an additive process during which the part is deposited layer by layer [2].

To deposit a part with designated geometric quality, a closed-loop process control system should be used. Laser metal deposition is a complex process, which is governed by a large number of parameters. Among these parameters, powder flow rate, laser power and travel speed are usually used to control the process properties, such as melt pool geometry, temperature, etc. Powder flow rate sensing and closed-loop control is implemented in [3] and [4]. Both controllers are capable of producing a steady powder flow rate. Heat input control in LMD is realized by adjusting laser power using an infrared image sensing camera as feedback [5]. The controller helps to overcome the effects of thermal variations and reduce cladding geometric variations. A PID controller is developed to control the clad height in [6]. The controller is designed based on a simplified process model. The laser power and powder flow rate are kept constant during the deposition, while the clad height is controlled by adjusting the travel speed. Except for those controllers mentioned above, which are based on deterministic process models, there are some other process controllers which are based on statistical models. Response surface models are developed to minimize the heat affected zone (HAZ) in [7].

Process control usually requires a process model. Different models are proposed to describe the LMD process. A lumped-parameter, analytical model of material and

thermal transfer is established in [8]. The model consists of three first order equations describing mass, momentum and energy balances. An elliptic shape melt pool is assumed. The model is validated by Gas Metal Arc Welding (GMAW) experiments through measurements by an infrared camera and a laser profilometry scanner. Another analytical model is developed and experimentally verified in [9]. The model concentrates on the mathematical analysis of the melt pool and establishes mass and energy balances based on one-dimensional heat conduction to the substrate. There are also some more complex models in the literature, such as the three dimensional model used to predict the thermal behavior and geometry of the melt pool in [10]. The Finite Element Method (FEM) is typically used to solve the equations in the complex models. The complex models usually require intense computational power, making them difficult to utilize in real time. The model complexity also hinders its usage for controller design.

The LMD process is dominated by a subtle energy balance, which is affected by the part and substrate geometries, ambient temperature, etc. Therefore LMD process is sensitive to environmental conditions. The model parameters change as the part is being built, making a constant parameter model implausible. Also, constant height is difficult to achieve. To accommodate these limitations, the layer-to-layer height control methodology is proposed. The idea of layer-to-layer height control is to measure the part height profile between different layers using a laser displacement sensor. The measured height profile and melt pool temperature are applied to identify the model parameters using PSO. The powder flow rate reference is then generated using ILC with respect to the reference height profile of the next layer. With the aid of layer-to-layer control, it is

possible to make the deposition process automatic, which will help to increase productivity and reduce cost.

This paper is organized as follows. Section 2 introduces the LMD system hardware. Section 3 formulates the process models and Section 4 presents the layer-to-layer height controller design. In Section 5 simulation and experimental results are presented and discussed. Finally, in Section 6, the paper is summarized and concluding remarks are presented.

2. Laser Metal Deposition System Hardware

The LMD system consists of the following components: 5-axis CNC machine, powder delivery system, 1kW diode laser, National Instruments (NI) real-time control system, laser displacement sensor and temperature sensor. The system setup is shown in Figure 1. The laser displacement sensor (OMRON, model Z4M-W100) has a measurement range of ± 40 mm and a minimum resolution of 8 μm. The temperature sensor (Mikron Infrared, model MI-GA 5-LO) has a measurement range of 400 to 2500°C. The temperature sensor is mounted on the nozzle and is used to measure the melt pool temperature during deposition. The entire control system is implemented in NI LabVIEW. The NI boards used in the system setup are listed in Table 1.

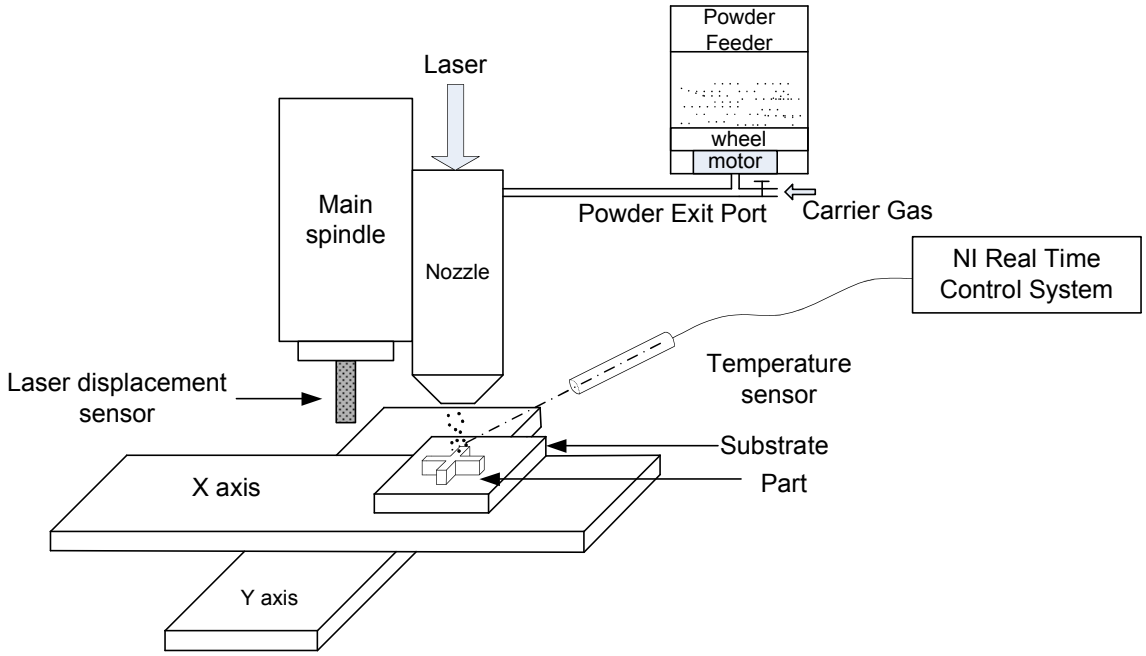

Figure 1: Laser metal deposition process system.

Table 1: NI boards used in the system setup.

Model	Type	Range	Resolution	Application
PXI-6602	Counter/Timer	N/A	N/A	Powder feeder motor angular position measurement
PXI-6040E	Analog input	-10V-+10V	12 bit (4.88 mV)	1. laser displacement sensor feedback measurement 2. temperature sensor feedback measurement
PXI-6711	Analog output	-10V-+10V	12 bit (4.88 mV)	1. powder feeder motor control 2. laser power control

3. Laser Metal Deposition Process Model

3.1 Model description

For on-line process control, a simplified model is more desirable due to its computation efficiency. The model [8] is composed of three equations derived from mass, momentum and energy balances.

The mass balance equation is given by

$$\rho \dot{V}(t) = -\rho A(t) v(t) + \mu_m m(t) \tag{1}$$

where ρ is material density (kg/m^3), V is bead volume (m^3), A is cross sectional area in the direction of deposition (m^2), v is table velocity in the direction of deposition (m/s), μ_m is powder catchment efficiency, and m is powder flow rate (kg/s). The bead is assumed to be elliptical; thus, the volume and cross sectional area in the direction of deposition, respectively, are

$$V(t) = \frac{\pi}{6} w(t) h(t) l(t) \tag{2}$$

$$A(t) = \frac{\pi}{4} w(t) h(t) \tag{3}$$

where w, h, l are, respectively, the bead width, height, and length (m).

The momentum balance equation is

$$\rho \dot{V}(t) v(t) + \rho V(t) \dot{v}(t) = -\rho \frac{\pi}{4} w(t) h(t) v(t) \left[-v(t)\right] + \alpha w(t) \tag{4}$$

where the parameter α is given by

$$\alpha = \left[1 - \cos(\theta)\right]\left[\gamma_{GL} - \gamma_{SL}\right] \tag{5}$$

where θ is the wetting angle (rad), γ_{GL} is the gas to liquid surface tension coefficient (N/m), and γ_{SL} is the solid to liquid surface tension coefficient (N/m).

The energy balance equation is

$$\begin{aligned}&\rho c_l \dot{T}(t) V(t) + \rho \dot{V}(t)\left[c_s\left(T_m - T_0\right) + h_{SL} + c_l\left(T(t) - T_m\right)\right] = \\ &-\rho \frac{\pi}{4} w(t) h(t) v(t) c_s\left(T_m - T_0\right) + \beta \mu_Q Q(t) - \frac{\pi}{4} w(t) l(t) \alpha_s\left(T(t) - T_m\right) \\ &-\left[\frac{\pi}{\sqrt[3]{2}}\left[w(t) h(t) l(t)\right]^{\frac{2}{3}}\right]\left[\alpha_G\left(T(t) - T_0\right) + \varepsilon\sigma\left(T^4(t) - T_0^4\right)\right]\end{aligned} \tag{6}$$

where T is the average melting pool temperature (K), c_s is the solid material specific heat (J/(kg·K)), T_m is the melting temperature (K), T_0 is the ambient temperature (K), h_{SL} is the specific latent heat of fusion-solidification (J/kg), c_l is the molten material specific heat (J/(kg·K)), β is the laser-surface coupling efficiency, μ_Q is the laser transmission efficiency, Q is the laser power (W), α_s is the convection coefficient (W/(m^2·K)), α_G is the heat transfer coefficient (W/(m^2·K)), ε is the surface emissivity and σ is the Stefan-Boltzmann constant (W/(m^2·K^4)).

The bead width-length relationship for the steady-state conductive temperature distribution subject to a heat source moving with constant velocity is given by

$$l(t) = X(t) + 0.25\frac{w^2(t)}{X(t)} \;\; with \;\; X(t) = \max\left[\frac{w(t)}{2}, \; \frac{\beta \mu_Q Q(t)}{2\pi k\left(T(t) - T_0\right)}\right] \tag{7}$$

where k is the thermal conductivity constant (W/(m·K)).

The experiments conducted in this paper use H13 tool steel as the deposition material. The model parameters for H13 tool steel are listed in Table 2 [9].

Table 2: **H13 properties and deposition conditions.**

Parameter	Symbol	Value
density (kg/m^3)	ρ	7760
wetting angle (rad)	θ	$\pi / 2$

gas to liquid surface tension coefficient (N/m)	γ_{GL}	1.94237
solid to liquid surface tension coefficient (N/m)	γ_{SL}	1.94246
solid material specific heat (J/(kg·K))	c_s	460
melting temperature (K)	T_m	1730
ambient temperature (K)	T_0	292
specific latent heat of fusion-solidification (J/kg)	h_{SL}	250000
molten material specific heat (J/(kg·K))	c_l	480
heat transfer coefficient (W/m^2·K)	α_G	24
surface emissivity	ε	0.53
Stefan-Boltzmann constant (W/m^2·K^4)	σ	$5.67\cdot10^{-8}$
thermal conductivity constant(W/m·K)	k	29
laser transmission efficiency	μ_Q	0.8
laser-surface coupling efficiency	β	0.15

3.2 Model Adaptation

Let $f = \dfrac{\beta\mu_Q Q(t)}{2\pi k\left(T(t)-T_0\right)}$, mathematical analysis shows that f is maximum when Q reaches maximum (1 kW) and T is minimum (1730 K). In this case, $f_{\max} = 4.58\cdot10^{-4} m$. Experiments show that the track width is close to the laser spot diameter, which is approximately $2.54\cdot10^{-3}$ (m) at nozzle standoff distance $1.27\cdot10^{-2}$ (m). Therefore equation (7) becomes

$$l(t) = w(t) \tag{8}$$

4 Laser Metal Deposition Height Controller Design

A height controller is designed based on the model described above. As shown in Figure 2, the height controller consists of three major parts: measurement (height and temperature), system identification, and powder flow rate reference generation. The height and temperature profiles are measured using the laser displacement and temperature sensors, respectively. The measurement data, together with the measured powder flow rate of the last layer, are used as inputs to the system identification program, which is based on PSO [11], to estimate model parameters. Since the estimated model parameters are only applicable to the deposition of the last layer, they are further predicted using EWMA so the model can be used to predict the deposition of the next layer. The powder flow rate reference profile, which will produce the designated layer height reference, is then generated using ILC.

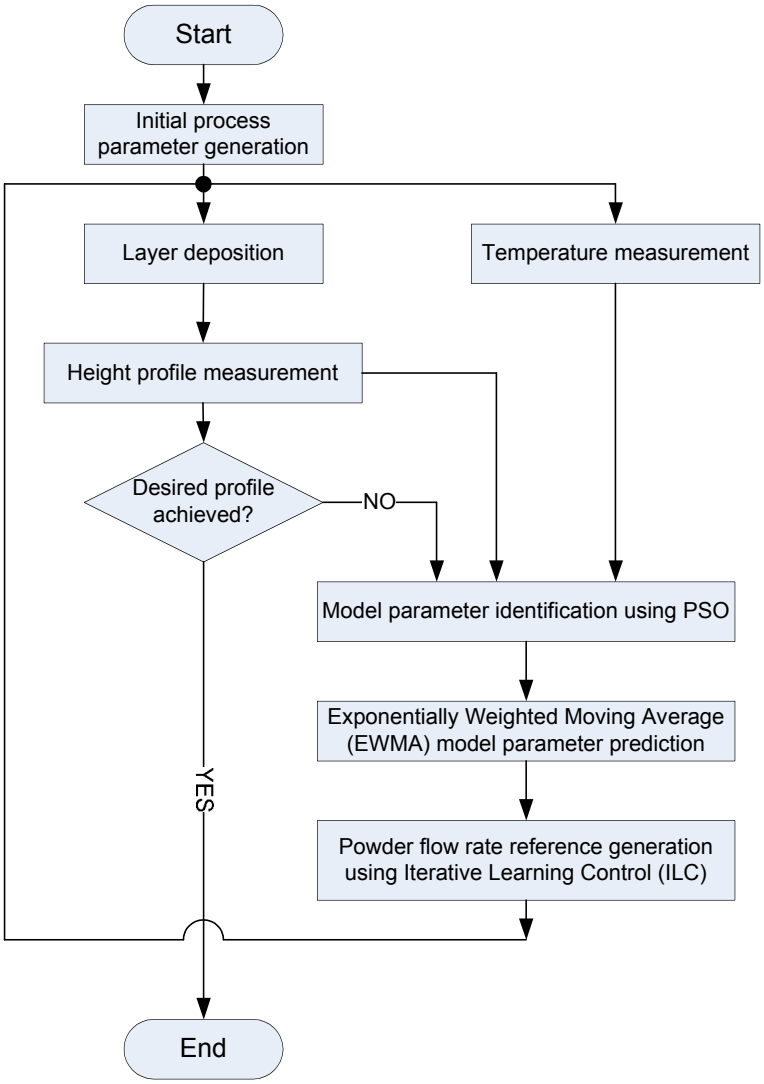

Figure 2: Laser metal deposition height controller structure.

4.1 System identification based on PSO

Particle swarm optimization is an evolutionary computational technique based on swarm intelligence. In the particle swarm algorithm, the trajectory of each particle (i.e., candidate solution to the optimization problem) in the search space is adjusted according to its own experience and the experience of the other particles in the swarm. It has been successfully applied in many different areas such as neural network training [12], system

modeling [13], engineering design [14], etc. In this paper, it is applied to estimate the model parameters based on measured height and temperature profiles. The LMD process is governed by a number of process parameters, among which heat transfer coefficient α_G, surface emissivity ε, thermal conductivity constant *k*, convection coefficient α_s and powder catchment efficiency μ_m, etc, are sensitive to the environment. Limited by the process feedback (height and temperature), only two process parameters, convection coefficient α_s (W/(m^2·K)) and powder catchment efficiency μ_m, are estimated.

The PSO algorithm is applied to determine the optimal values of α_s and μ_m based on the height and temperature feedback. Assume the swarm consists of *n* particles and the position and velocity vectors of particle *i* can be represented as $X_i = [\alpha_{si}, \mu_{mi}]$, $i = 1, 2, \cdots, n$ and $V_i = \left[v_{\alpha_s i}, v_{\mu_m i} \right]$, $i = 1, 2, \cdots, n$, respectively. The position vector represents the current solution found by each particle, while the velocity vector shows how the solution will change in the next iteration.

The steps of the identification algorithm are as follows:

(1) Randomly initialize the position and velocity vectors of particle *i* as $X_i(0) = [\alpha_{si}(0), \mu_{mi}(0)]$ and $V_i(0) = \left[v_{\alpha_s i}(0), v_{\mu_m i}(0) \right]$, $i = 1, 2, \cdots, n$, respectively, and compute the fitness *J* of each particle by comparison of the height and temperature feedback with the deposition process simulation results using the Runge-Kutta method. In this paper, the fitness *J* is calculated by the following equation

$$J = \sum_{j=1}^{q} w_h \cdot \left(h_m(j) - h_s(j) \right)^2 + \sum_{j=1}^{q} w_T \cdot \left(T_m(j) - T_s(j) \right)^2 \tag{9}$$

where q is the total sample number, w_h is weight on height error, h_m is the measured height, h_s is the simulated height, w_T is the weight on temperature error, T_m is the measured temperature and T_s is the simulated temperature. Take the current position of each particle as its initial personal best position $P_i(0)$ with best fitness $JPbest_i(0)$, $i=1,2,\cdots,n$, and compare the fitness of all particles in the group to find the initial global best position $P_g(0)$ and corresponding initial global best fitness $JGbest(0)$.

(2) Update the current iteration number b and inertial weight with $w(b)$

$$b=b+1,\quad w(b)=w_i-\left(\frac{w_i-w_f}{b_{\max}}\right)\cdot b \tag{10}$$

where $b_{\max}$ is the maximum iteration number. The initial and final values of the inertia weight, respectively, are 0.9 and 0.4.

(3) Update the position and velocity of each particle

$$V_i(b+1)=w(b)V_i(b)+c_1r_1\left(P_i(b)-X_i(b)\right)+c_2r_2\left(P_g(b)-X_i(b)\right),\quad i=1,2,\cdots,n \tag{11}$$

$$X_i(b+1)=X_i(b)+V_i(b+1),\quad i=1,2,\cdots,n \tag{12}$$

The acceleration coefficients c_1 and c_2, respectively, are 0.2 and 0.2. The parameters r_1 and r_2 are random numbers in the range [0,1].

(4) Evaluate the fitness of each particle $J_i(b)$, and compare it with its previous personal best fitness value $JPbest_i(b-1)$. If $J_i(b)<JPbest_i(b-1)$, then $P_i(b)=X_i(b)$ and $JPbest_i(b)=J_i(b)$. Compare $J_i(b)$ with the previous global

best fitness $JGbest(b-1)$. If $J_i(b) < JGbest(b-1)$, then $P_g(b) = X_i(b)$ and $JGbest(b) = J_i(b)$.

(5) Compare $JGbest(b)$ with $JGbest(b-1)$. If $JGbest(b) = JGbest(b-1)$, then let $c = c+1$; If $JGbest(b) \neq JGbest(b-1)$, the $c = 0$. If $c > C_{set}$, then randomly select $\delta(\leq n)$ particles from the group and reinitialize. Here C_{set} is a designated natural number. If there is no fitness improvement in the past C_{set} iterations, the reinitializing process will be activated.

(6) If $b < b_{\max}$, then go to step (2), otherwise stop.

Similar to other optimization algorithms such as genetic algorithm, simulated annealing, etc., PSO can also become trapped at a local minimum. Here step (5) is employed to avoid local minima. The idea originates from the mutation operation used in genetic algorithms. In genetic algorithms, mutation is a random modification of a randomly selected potential solution. It guarantees the possibility of exploring the space of solutions for any initial solution space and avoiding local minima. Here the reinitializing process is designed to fulfill the same purpose.

4.2 Model parameters prediction using EWMA

With PSO algorithm described above, the parameters, α_s and μ_m, can be estimated for the current layer, but they are not applicable to the deposition of next layer. To predict the parameter value for the next layer, Exponentially Weighted Moving Average (EWMA) can be used. The prediction is described by

$$P_{l+1} = A \cdot E_l + (I - A) \cdot P_l,\ l = 2, \cdots \tag{13}$$

$$P_2 = E_1 \tag{14}$$

where l is the layer number, the vector of predicted parameters at layer l+1, $P_{l+1} = \left[\alpha_{sp}(l+1), \mu_{mp}(l+1)\right]$, the vector of estimated parameters using PSO at layer l, $E_l = \left[\alpha_{se}(l), \mu_{me}(l)\right]$, I is a 2×2 identity matrix, A is a 2×2 diagonal matrix constituted by smooth factors for each parameter, here $A = \begin{bmatrix} 0.5 & 0 \\ 0 & 0.5 \end{bmatrix}$.

4.3 Powder Flow Rate Generation using ILC

Iterative Learning Control (ILC) has been widely applied in robotics for tracking repeated motion contours. The idea is to adjust the controller output according to the tracking error in the previous iterations and, since the motions are usually repeated, the controller output will converge to a certain value which will produce an acceptable tracking result. The control law is

$$u_{j+1}(i) = f\left(e_j, e_{j-1}, \cdots, e_{j-n}, u_j, \cdots, u_{j-n}\right) \tag{15}$$

so that the learning convergence, i.e., $\lim_{j\to\infty}\left\|e_j\right\| \to 0$ and $\lim_{j\to\infty}\left\|u^* - u_j\right\| \to 0$ is achieved at an acceptable rate. The parameter j is the iteration number, and i is the sample index.

Unlike its most usual application described above, ILC is used to generate the powder flow rate reference profile in this paper. The control law applied in this paper is first proposed by Arimoto *et al*.[15] and is

$$m_{j+1}(i) = m_j(i) + \gamma e_j(i+1) \tag{16}$$

The powder flow rate of time i at iteration j+1 is calculated from the powder flow rate of time i at the previous iteration j and a corrective term which is a learning gain γ

multiplied by the shifted tracking error $e_j(i+1)$ from the previous iteration. The procedure is given in Figure 3. One thing that should be noted is that in this procedure ILC utilizes virtual deposition (with the help of process model) to generate the powder flow rate reference.

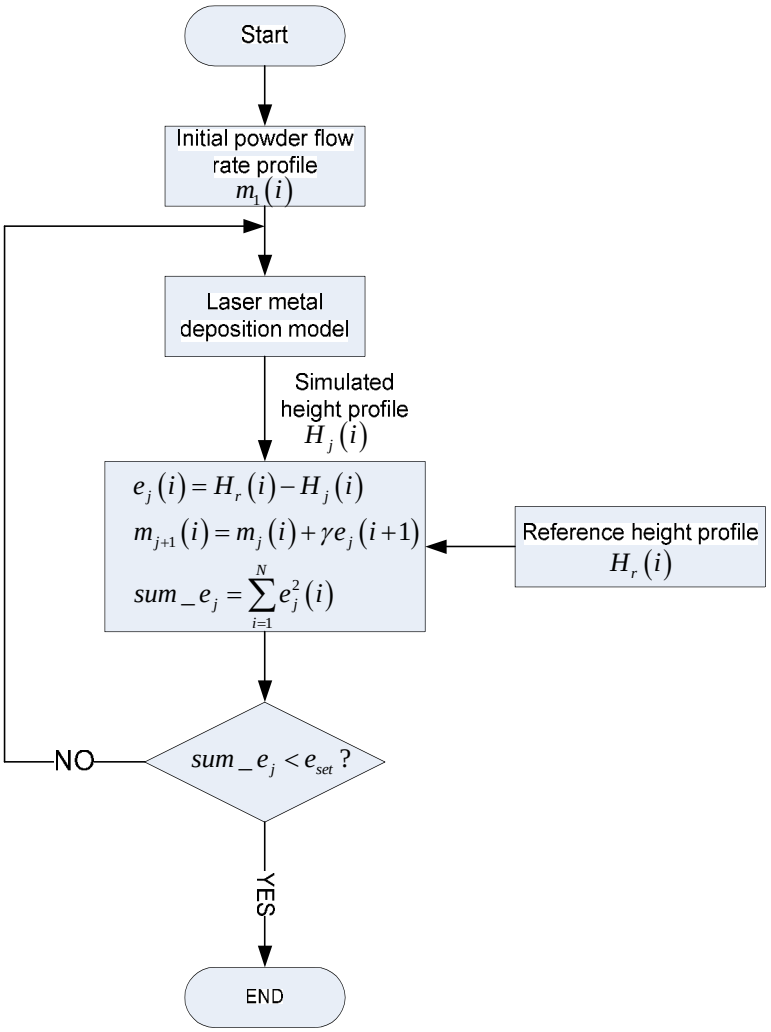

Figure 3: Reference powder flow rate profile generation using ILC.

5 Experiments and Simulation Studies

5.1 Process model parameter estimation

To test the model parameter identification methodology, a four-layer single track wall is deposited using H13. The process parameters are listed in Table 3.

Table 3: Model parameter estimation experimental process parameters.

Parameter	Powder flow rate (kg/s)	Laser power (W)	Table travel velocity (m/s)	Nozzle standoff distance (m)
Value	$0.83 \cdot 10^{-4}$	700	$2.1 \cdot 10^{-3}$	$1.27 \cdot 10^{-2}$

The track length is approximately 60 (mm). The measured track height and melt pool temperature are shown in Figure 4.

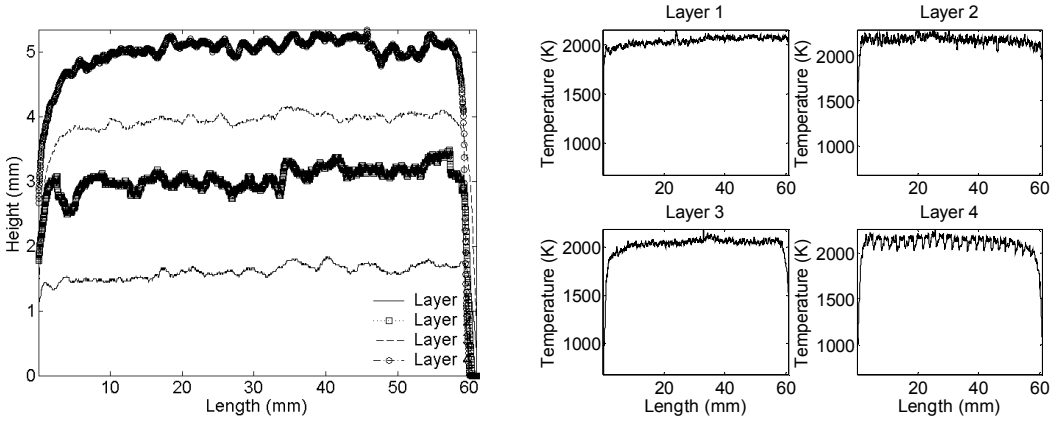

Figure 4: Measured track height and temperature profiles for four layers.

The model parameters (α_s and μ_m) are estimated using PSO algorithm for all four layers. The estimated parameter values are given in Table 4.

Table 4: Estimated model parameters for all four layers.

Parameter	convection coefficient α_s (W/m^2·K)	powder catchment efficiency μ_m

Layer 1	$2.46 \cdot 10^4$	0.62
Layer 2	$1.87 \cdot 10^4$	0.56
Layer 3	$3.55 \cdot 10^4$	0.35
Layer 4	$2.59 \cdot 10^4$	0.43

The experimental results are compared with the simulation results in Figure 5. The results show that the simulation results using estimated parameters match the experimental results quite well except for the variations, which are due to unmodeled process dynamics. The other thing that should be noted is that parameters experience significant changes between layers indicating the necessity of parameter prediction.

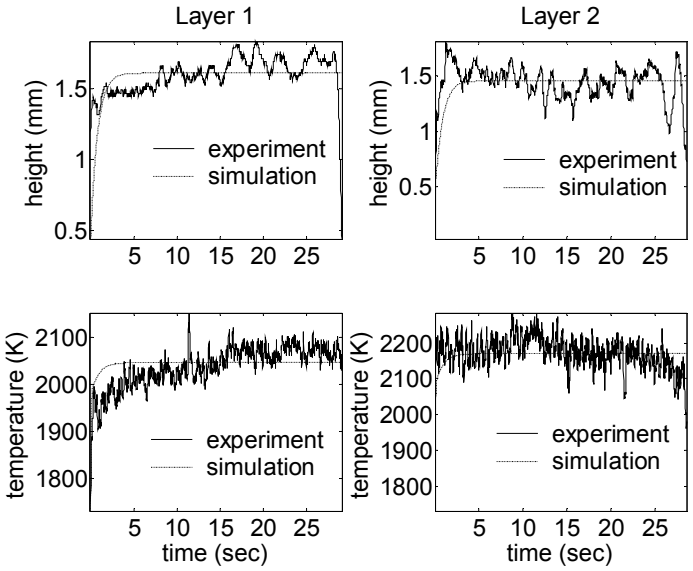

Figure 5: Experimental and simulation results comparison (Layer 1 and Layer 2).

5.2 Powder Flow Rate Reference Generation Simulation Study

The powder flow rate reference generation methodology presented above is applied to a circular part deposition. The velocity (along deposition path) profile recorded from the

execution of a clockwise circle (R = 25.4 mm, V = 254 mm/min) on the CNC machine is shown in Figure 6.

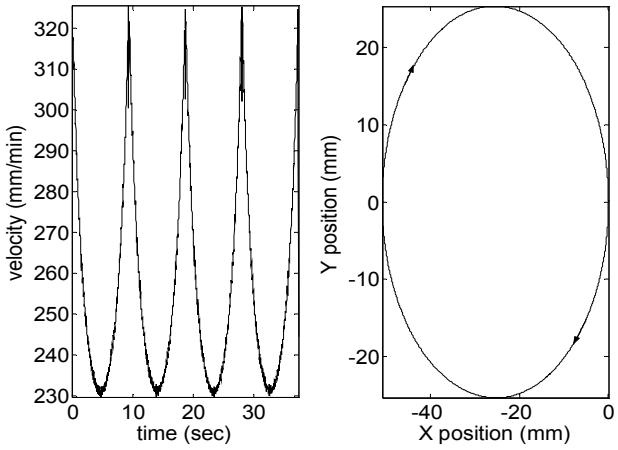

Figure 6: Measured velocity profile from execution of a clockwise circle (R = 25.4 mm, V = 254 mm/min) on CNC machine.

The model parameters estimated for Layer 4 in above experiment are employed to conduct the simulation. The height reference is set to 0.6 mm. The initial powder flow rate is set to 5 g/min. Learning gain of ILC is 0.04. The ILC program runs on the computer platform with the following settings: CPU – Celeron M (1.40 GHz), Memory – 448 MB, System – Windows XP home edition (2002). The total iteration number is 200 and the computation time is 3.60 s. The simulation results are shown in Figure 7.

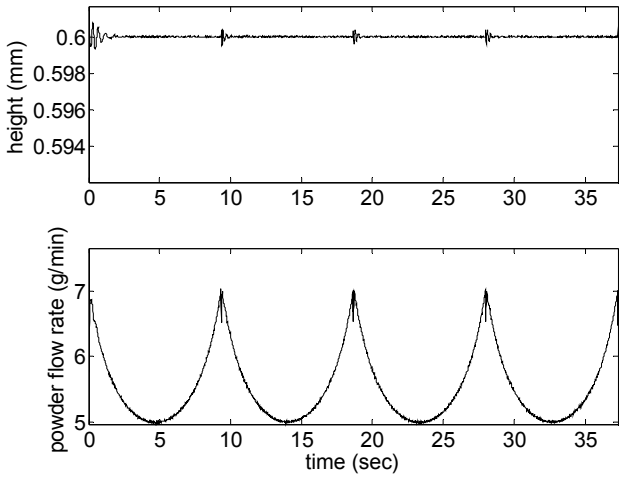

Figure 7: Layer height and corresponding powder flow rate profile.

It could be seen that with the powder flow rate reference generated by the ILC program, the layer height is approximately 0.6 mm. The small glitches on the height profile are due to the sharp velocity changes.

6 Summary and Conclusions

A LMD height controller design methodology is presented in this paper. The height controller utilizes the PSO algorithm to estimate the model parameters from measured temperature and track height profiles between layers. The model parameters are then further predicted using EWMA to account for the process parameter variations. With the predicted model, the powder flow rate reference profile, which will produce the designated layer height profile, is then generated using ILC. The model estimation capability of the methodology is verified experimentally. Simulation study shows that the methodology works well in producing the reference layer height.

7. Acknowledgment

This research was supported by the Intelligent Systems Center at Missouri S&T.

Reference

[1] Choi, J., 2002, "Process and Prosperities Control in Laser Aided Direct Metal/Materials Deposition Process," *Proceedings of IMECE*, New Orleans, Louisiana, November 17–22, pp. 1–9.

[2] Griffith, M.L., Keicher, D.M., Atwood C.L., Romero J.A., Smegeresky J.E., Harwell L.D., and Greene D.L., 1996, "Free Form Fabrication of Metallic Components Using Laser Engineered Net Shaping (LENS)," *Solid Freeform Fabrication Symposium*, Austin, Texas, pp. 125–131.

[3] Hu, D. and Kovacevic, R., 2003, "Sensing, Modeling and Control for Laser–Based Additive Manufacturing," *International Journal of Machine Tools and Manufacture*, Vol. 43, No. 1, pp. 51–60.

[4] Li, L. and Steen, W.M., 1993, "Sensing, Modeling and Closed Loop Control of Powder Feeder for Laser Surface Modification," *ICALEO*, pp. 965–975.

[5] Hu, D., Mei H., and Kovacevic R., 2001, "Closed Loop Control of 3D Laser Cladding Based on Infrared Sensing," *Solid Freeform Fabrication Proceedings*, Austin, Texas, pp. 129–137.

[6] Fathi A., Durali M., Toyserkani, E., and Khajepour, A., 2006, "Control of the Clad Height in Laser Powder Deposition Process using a PID Controller," *Proceedings of IMECE*, November 5–10, Chicago, Illinois, USA.

[7] Keicher, D.M., Jellison, J.L., Schanwald, L.P., Romero, J. A., and Abbott, D.H., 1995, "Towards a Reliable Laser Spray Powder Deposition System through Process Characterization," 27th *International SAMPE Technical Conference*, October 9–12, pp. 1009–1018.

[8] Doumanidis C. and Kwak, Y-M., 2001, “Geometry Modeling and Control by Infrared and Laser Sensing in Thermal Manufacturing with Material Deposition,” *Journal of Manufacturing Science and Engineering*, Vol. 123, pp. 45–52.

[9] Han L., Liou, F.W., and Musti S., 2005, “Thermal Behavior and Geometry Model of Melt Pool in Laser Material Process,” *Journal of Heat Transfer*, Vol. 127, pp. 1005–1014.

[10] Pinkerton A.J. and Li L., 2004, “Modelling the Geometry of a Moving Laser Melt Pool and Deposition Track via Energy and Mass Balances,” *Journal of Physics D: Applied Physics*, Vol. 37, pp. 1885–1895.

[11] Kennedy J. and Eberhart R.C., 1995, “Particle Swarm Optimization,” *IEEE International Conference on Neural Networks*, Perth, Australia, November, pp. 1942–1948.

[12] Gudise, V.G. and Venayagamoorthy, G.K., 2003, “Comparison of Particle Swarm Optimization and Back Propagation as Training Algorithms for Neural Networks,” *IEEE Swarm Intelligence Symposium*, pp. 110–117.

[13] Bhattacharya, R., Joshi, A. and Bhattacharya, T.K., 2006, “PSO-based Evolutionary Optimization for Black-box Modeling of Arbitrary Shaped on-chip RF Inductors,” *Silicon Monolithic Integrated Circuits in RF Systems, Digest of Papers*, pp. 103–106.

[14] Hu X., Eberhart, R.C. and Shi Y., 2003, “Engineering Optimization with Particle Swarm,” *IEEE Swarm Intelligence Symposium*, pp. 53–57.

[15] Arimoto, S., Kawamura, S., and Miyazaki, F., 1984, “Bettering Operations of Robots by Learning,” *Journal of Robotic Systems*, Vol. 1, pp. 123–140.